

## THE STRUCTURE OF THE HOMUNCULUS. I. SHAPE AND LATITUDE DEPENDENCE FROM H<sub>2</sub> AND [Fe II] VELOCITY MAPS OF $\eta$ CARINAE<sup>1</sup>

NATHAN SMITH<sup>2</sup>

Center for Astrophysics and Space Astronomy, University of Colorado, 389 UCB, Boulder, CO 80309; nathans@casa.colorado.edu

Received 2006 January 31; accepted 2006 February 17

### ABSTRACT

High-resolution long-slit spectra obtained with the Phoenix spectrograph on Gemini South provide our most accurate probe of the three-dimensional structure of the Homunculus Nebula around  $\eta$  Carinae. The new near-infrared spectra dramatically confirm the double-shell structure inferred previously from thermal dust emission, resolving the nebula into a very thin outer shell seen in H<sub>2</sub> and a warmer, thicker inner layer seen in [Fe II]. The remarkably thin and uniform H<sub>2</sub> skin hints that the most important mass loss during the 19th century eruption had a very short duration of  $\lesssim 5$  yr. H<sub>2</sub> emission traces the majority of the more than  $10 M_{\odot}$  of material in the nebula and has an average density of order  $n_{\text{H}} \gtrsim 10^{6.5} \text{ cm}^{-3}$ . This emission, in turn, yields our first definitive picture of the exact shape of the nebula, plus a distance of  $2350 \pm 50$  pc and an inclination angle of  $\sim 41^{\circ}$ . The distribution of the H<sub>2</sub> emission provides the first measure of the latitude dependence of the speed, mass loss, and kinetic energy associated with  $\eta$  Car's 19th century explosion. Almost 75% of the total mass and more than 90% of the kinetic energy in the ejecta were released at high latitudes between  $45^{\circ}$  and the polar axis. This rules out a model for the bipolar shape in which an otherwise spherical explosion was pinched at the waist by a circumstellar torus. Instead, most of the mass appears to have been directed poleward by the explosion itself. H<sub>2</sub> emission also provides our first reliable picture of the critical innermost waist of the Homunculus, yielding clues to the observed morphology of the core and the more extended equatorial debris.

*Subject headings:* circumstellar matter — ISM: individual (Homunculus Nebula) — stars: individual ( $\eta$  Carinae) — stars: mass loss — stars: winds, outflows

### 1. INTRODUCTION

The Homunculus Nebula around  $\eta$  Carinae is composed of a striking pair of lumpy bipolar lobes divided by a ragged equatorial skirt (Morse et al. 1998; Duschl et al. 1995; Smith et al. 2000; Smith & Gehrz 2000). It is primarily a reflection nebula at UV, visual, and near-IR wavelengths, since it is highly polarized (Thackeray 1956b, 1961; Visvanathan 1967; Meaburn et al. 1993; Schulte-Ladbeck et al. 1999), and because stellar wind emission lines are seen reflected by the nebula (Allen & Hillier 1991; Davidson et al. 1995; Smith et al. 2003a; Stahl et al. 2005). While spectacular in appearance, scattered-light images do not give a clear picture of the three-dimensional (3D) shape, tilt angle, or detailed structure of the nebula because the optical depth is near unity and the inclination angle hides parts of the nebula. In addition, the underlying structure giving rise to the clumpy, mottled appearance of the polar lobes in *Hubble Space Telescope* (HST) and infrared (IR) images defies easy explanation. Different data sets imply different mass distributions in dark lanes, holes, and bright cells or clumps (e.g., Morse et al. 1998; Smith et al. 1998), evoking entertaining comparisons to structures seen in convection cells and vegetables.

Because of its prominence and a wealth of high-quality observational data, the Homunculus is an important prototype of bipolar nebulae, being the focus of numerous theoretical studies (Frank et al. 1995, 1998; Owocki & Gayley 1997; Dwarkadas & Balick 1998; Langer et al. 1999; Dwarkadas & Owocki 2002;

Owocki 2003; Soker 2001, 2004; Matt & Balick 2004; Gonzalez et al. 2004a, 2004b). Yet, the formation of its clumpy bipolar lobes remains an enduring mystery. Even more perplexing is its ragged equatorial disk, which makes the Homunculus unique among bipolar nebulae (Davidson et al. 1997, 2001; Zethson et al. 1999; Smith & Gehrz 1998; Smith et al. 1998, 2002). Detailed study of this nebula provides one of our most valuable ways to learn about the Great Eruption of  $\eta$  Carinae in the mid-19th century, since proper motions indicate that the nebula was ejected in that event (Gaviola 1950; Ringuélet 1958; Currie et al. 1996; Smith & Gehrz 1998; Morse et al. 2001). An important observational goal is to measure the exact shape and mass distribution in the nebula, because it bears the direct imprint of the physics of the Great Eruption as a function of latitude. This, in turn, can constrain the roles of rotation, binarity, and the hydrodynamics of interacting winds in the formation of bipolar structure.

Thermal-IR observations have yielded important clues about the structure of the Homunculus, because the nebula is optically thin at these wavelengths (they have also provided our best estimates of its total mass of more than  $10 M_{\odot}$  and IR luminosity of  $4.3 \times 10^6 L_{\odot}$ ; Smith et al. 2003b). Mid-IR maps by Hackwell et al. (1986) first revealed that the bipolar nebula consisted of a pair of hollow, limb-brightened osculating spheroids. This basic structure was later supported by a much higher resolution monochromatic  $12 \mu\text{m}$  image (Smith et al. 1995), multiwavelength mid-IR images (Smith et al. 1998; Polomski et al. 1999), mid-IR imaging polarimetry (Aitken et al. 1995), and spectroscopy (Hillier & Allen 1992; Meaburn et al. 1993). While the Homunculus had roughly the same size in thermal emission from 8 to  $13 \mu\text{m}$ , Smith et al. (1998) noted that it was considerably larger in scattered light images at  $\lambda < 2 \mu\text{m}$ . This mystery was resolved with higher resolution thermal-IR imaging using larger telescopes. Smith et al. (2003b) used images from the Magellan Observatory to demonstrate that the nebula was also larger at  $18\text{--}25 \mu\text{m}$  than at

<sup>1</sup> Based on observations obtained at the Gemini Observatory, which is operated by AURA, Inc., under a cooperative agreement with the NSF on behalf of the Gemini partnership: the National Science Foundation (USA), the Particle Physics and Astronomy Research Council (UK), the National Research Council (Canada), CONICYT (Chile), the Australian Research Council (Australia), CNPq (Brazil), and CONICET (Argentina).

<sup>2</sup> Hubble Fellow.

8–13  $\mu\text{m}$ . In that paper, we proposed a *double-shell structure* for the polar lobes, in which a warm ( $\sim 200$  K) inner shell dominates the 8–13  $\mu\text{m}$  images, and a cooler ( $\sim 140$  K) outer skin dominates at longer wavelengths. The double-shell structure will be an important recurring theme in the present investigation. This model also indicated that most of the greater than  $10 M_{\odot}$  in the Homunculus was associated with the cool outer skin of the polar lobes, settling an earlier debate about the origin of the far-IR emission from  $\eta$  Car (Davidson & Smith 2000; Morris et al. 1999). Thermal-IR maps show complex dust structure in the homunculus core as well (Smith et al. 1995, 2002; Chesneau et al. 2005), which is discussed in detail at the end of this paper.

Since the Homunculus is essentially a ballistic expanding Hubble flow, measured Doppler shifts in the ejecta provide another viable method to trace the 3D shape. Several authors have used this technique with spectroscopy of visual-wavelength emission lines (Thackeray 1951, 1956a, 1956b, 1961; Meaburn et al. 1987, 1993; Hillier & Allen 1992; Allen & Hillier 1991, 1993; Currie et al. 1996; Meaburn 1999), as well as imaging polarimetry (Schulte-Ladbeck et al. 1999). However, none of these various studies gave a definitive measure of the shape, largely due to the low spatial resolution of ground-based spectroscopy, plus the very bright scattered continuum light and high optical depth of the dusty nebula at visual wavelengths (see Hillier 1997 for a review of proposed model shapes). This situation improved significantly when high spatial resolution optical spectra from the Space Telescope Imaging Spectrograph (STIS) became available. Davidson et al. (2001) studied the kinematic structure of narrow [Ni II] and [Fe II] emission lines in STIS spectra to give the first clear picture of the shape of the polar lobes and their inclination angle, plus the first genuine detection of the thin equatorial disk. However, our major result in that study was still rather unsatisfying; our model shape that best fit the kinematic data (“model 1” of Davidson et al. 2001) yielded a projected image of the polar lobes that was *far too small and skinny* to explain images of the Homunculus. We see below that the solution to this mystery is that the [Ni II] and [Fe II] lines studied at visual wavelengths actually trace a smaller inner shell of the polar lobes and not the dominant outer layer of the Homunculus seen in images.

The discovery of molecular gas in the Homunculus (Smith 2002a; Smith & Davidson 2001) provided a powerful new tool to study its structure via near-IR emission from  $\text{H}_2 v = 1-0 S(1) \lambda 21218$ . This emission line is bright and narrow, is only seen in intrinsic emission from the polar lobes (no confusing reflected emission), and is at a wavelength of  $\sim 2 \mu\text{m}$  where we can begin to see through to the back of the Homunculus. Hence, spectra of  $\text{H}_2$  revealed emission from the far side of the Homunculus lobes for the first time (Smith 2002a). Smith (2002a) showed that the  $\text{H}_2$  emission most likely originates in an outer shell, separate from the inner [Fe II] shell. Thus,  $\text{H}_2$  probably traces gas associated with the same outer cool dust shell seen in thermal-IR images (Smith et al. 2003b). It is therefore our most powerful kinematic diagnostic of the majority of the mass in the Homunculus and traces the component of the nebula that dominates images. However, earlier [Fe II] and  $\text{H}_2$  spectra had inadequate spectral resolution to clearly discern the relative thickness of the two shells or their detailed structure. The present study aims to rectify this situation using long-slit spectra of  $\text{H}_2$  and [Fe II] obtained with much higher dispersion.

## 2. OBSERVATIONS

High-resolution ( $R \simeq 60,000$ ;  $\sim 5 \text{ km s}^{-1}$ ) near-IR spectra of  $\eta$  Car were obtained on 2005 March 1 and 2 using the Phoenix spectrograph (Hinkle et al. 2003) on the Gemini South telescope.

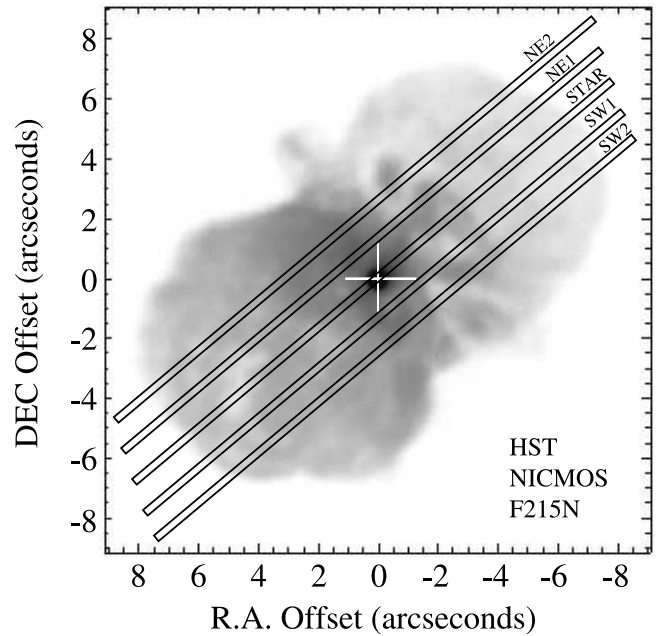


FIG. 1.—Phoenix slit aperture positions superposed on a  $2 \mu\text{m}$  *HST*/NICMOS image of  $\eta$  Car from Smith & Gehrz (2000).

Phoenix has a  $1024 \times 256$  InSb detector with a pixel scale of  $0''.085 \times 1.4 \text{ km s}^{-1}$  at a wavelength of  $\sim 1.6 \mu\text{m}$  and  $1.26 \text{ km s}^{-1}$  at  $\sim 2 \mu\text{m}$ . Sky conditions were photometric, and the seeing was typically  $0''.3$ – $0''.5$  (better at the longer wavelength). Removal of airglow lines was accomplished by subtracting an observation of an off-source position  $35''$  southeast of the star. The  $0''.25$  wide long-slit aperture was oriented at P.A. =  $310^\circ$  along the polar axis of the Homunculus. To sample the kinematics across the nebula, the slit was positioned on the bright central star, plus offsets of  $1''$  and  $2''$  in either direction perpendicular to the slit axis as shown in Figure 1. The observations were very similar to those described in earlier papers presenting Phoenix data (Smith 2004, 2005).

HR 3685 and HR 4621 were observed with Phoenix on the same nights with the same grating settings in order to correct for telluric absorption and for flux calibration. Telluric lines were used for wavelength calibration, using the telluric spectrum available from NOAO. Velocities were calculated adopting a vacuum rest wavelength of  $16439.981 \text{ \AA}$  for the [Fe II] ( $a^4F - a^4D$ ) line and  $21218.356 \text{ \AA}$  for  $\text{H}_2 v = 1-0 S(1)$ . These velocities were corrected to a heliocentric reference frame; heliocentric velocities are quoted here. Uncertainty in the resulting velocities is  $\pm 1 \text{ km s}^{-1}$ , dominated by scatter in the dispersion solution for telluric lines.

At all five slit placements, long-slit spectra were obtained for the two emission lines, [Fe II]  $\lambda 16435$  and  $\text{H}_2 \lambda 21218$ . These were suspected to be the most unambiguous tracers of the structure in the polar lobes of the Homunculus at near-IR wavelengths that can penetrate the dusty nebula (Smith 2002a). The Phoenix slit is shorter than the  $\sim 18''$  extent of the Homunculus, so each offset position in Figure 1 actually consisted of exposures at three steps along the slit that were shifted and combined later to yield a greater effective slit length. At each pointing two or three exposures, each consisting of  $2 \times 60$  s integrations (to avoid severe saturation), were obtained. Depending on the overlap at various positions along the slit, the total effective integration time after adding all exposures for a given slit position varied from 240 to 1080 s. Earlier experience with Phoenix (Smith 2004, 2005)

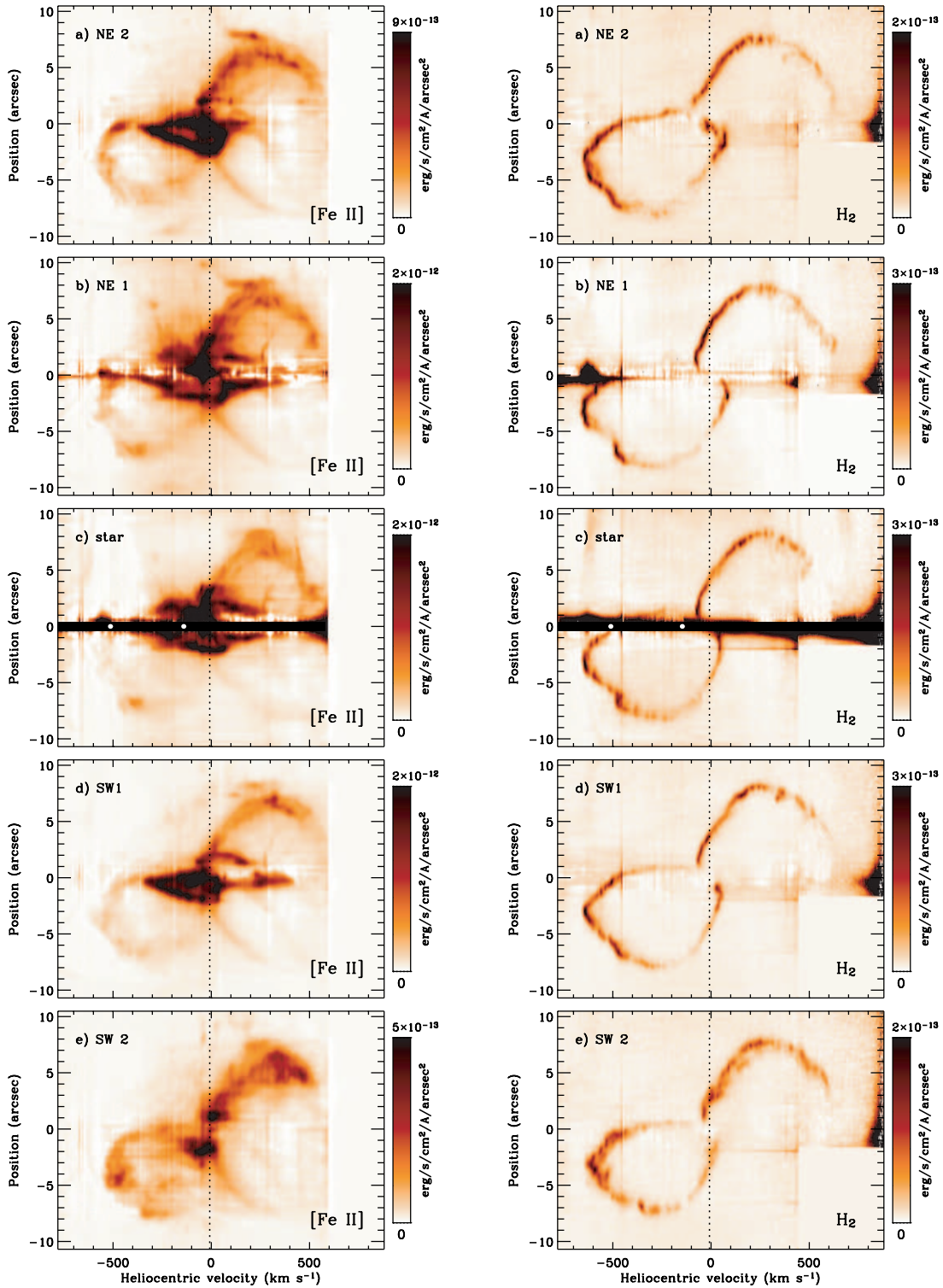


FIG. 2.—Kinematic structure of  $[\text{Fe II}] \lambda 16435$  emission (*left*) and  $\text{H}_2 v = 1-0 S(1) \lambda 21218$  emission (*right*), corresponding to the five different slit positions in Fig. 1. Reflected continuum emission has been subtracted with a linear fit, but some residuals remain, especially near the bright central star. The dashed line shows the systemic velocity of  $-8.1 \text{ km s}^{-1}$  (heliocentric). Small white dots in slits passing through the central star mark the  $-513$  and  $-146 \text{ km s}^{-1}$  absorption components seen in UV spectra.

revealed that the maximal extent of the blue and redshifted  $\text{H}_2$  velocities in the Homunculus reached slightly beyond the usable bandwidth of a single Phoenix exposure. Therefore, for  $\text{H}_2$  emission, observations were obtained at two different grating settings separated by about  $400 \text{ km s}^{-1}$ ; one optimized for including the structure of the blueshifted polar lobe and one for the redshifted lobe. The exposures at the redshifted setting were then scaled to

have exactly the same dispersion per pixel and combined with the blueshifted data. (Since the extreme redshifted velocities are only seen in the northwest polar lobe, the southeast pointings along the slit were ignored. This explains the data gap in the lower right corner of each panel on the right side of Fig. 2.)

Figure 2 shows the resulting long-slit data for  $[\text{Fe II}]$  and  $\text{H}_2$ , respectively, at the five different slit positions, where a linear fit

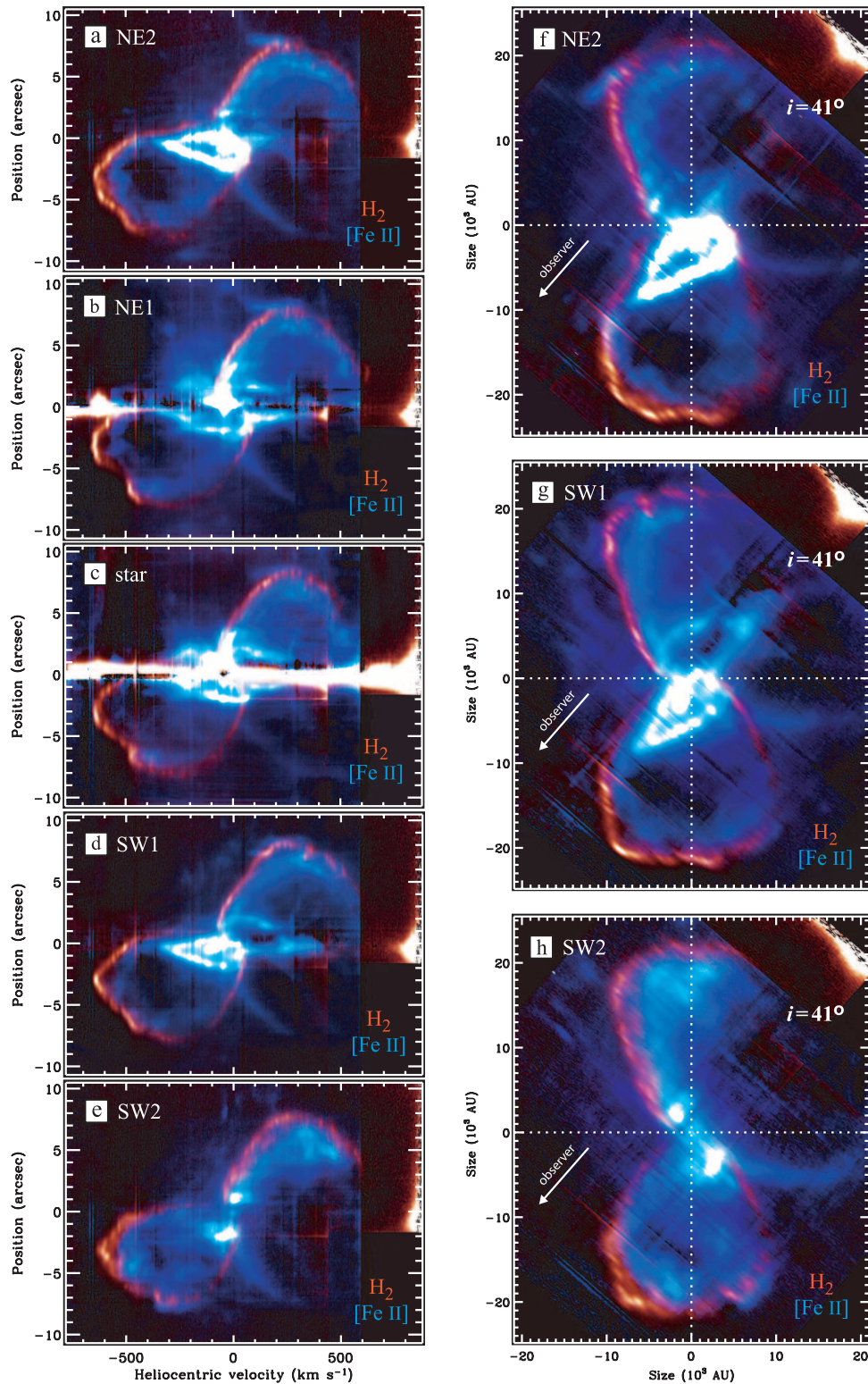


FIG. 3.—(a–e) Same as Fig. 2, but showing both [Fe II]  $\lambda 16435$  (blue) and  $\text{H}_2 v = 1-0S(1) \lambda 21218$  (red) simultaneously. Panels *f*, *g*, and *h* show the data from panels *a*, *d*, and *e*, respectively, but with the velocity and spatial scales converted to AU (assuming an age of 160 yr and a distance of 2350 pc), and rotated to correct for an inclination of  $i = 41^\circ \pm 0^\circ.5$ .

to the bright reflected continuum light in the Homunculus has been subtracted out to enhance the contrast of the line emission (see Smith 2002a, 2004, 2005 for more details). The vertical dashed lines in Figure 2 mark the systemic velocity of  $\eta$  Car at  $-8.1 \text{ km s}^{-1}$ , measured from earlier Phoenix spectra of  $\text{H}_2$  in the Homunculus (Smith 2004).

### 3. THE DOUBLE-SHELL MORPHOLOGY

Three distinct kinematic components can be seen in Figures 2 and 3, (1) a thin outer shell of  $\text{H}_2$  at  $\pm 600 \text{ km s}^{-1}$  and  $\pm 8''$ , (2) a thicker inner skin of [Fe II] at  $\pm 500 \text{ km s}^{-1}$  and  $\pm 8''$ , and (3) [Fe II] emission at  $\pm 250 \text{ km s}^{-1}$  and  $\pm 2''$  from the smaller

bipolar nebula known as the “Little Homunculus,” which was the subject of a previous paper (Smith 2005).<sup>3</sup>

It is clear from Figure 3 that  $H_2$  and  $[Fe\ II]$  emission in the polar lobes do not share the same spatial distribution. In fact, they are strongly anticorrelated. The observed kinematic structure gives a dramatic and independent confirmation of the double-shell structure proposed initially from thermal-IR images (Smith et al. 2003b), consisting of a warm inner dust shell, plus a cooler and denser outer shell. Here, the  $[Fe\ II]$  emission clearly traces the warmer inner shell, while the  $H_2$  emission corresponds to the more massive thin outer skin.

### 3.1. The Inner $[Fe\ II]$ Shell

$[Fe\ II]$  emission in Figures 2 and 3 coincides with the warmer inner dust shell of the polar lobes and therefore traces only about 10% of the total mass in the Homunculus (Smith et al. 2003b). For this reason, the main focus of the present paper is on the  $H_2$  emission. However, a few comments are in order, as the kinematic structure of the inner  $[Fe\ II]$  shell is closely related to the more massive cool  $H_2$  skin.

At all latitudes  $[Fe\ II]$  emission from the lobes has a smaller radius than the  $H_2$  emission and clearly represents a separate component of the nebula. The infrared  $[Fe\ II]$  emission shown here is emitted by the same gas that gives rise to optical  $[Ni\ II]$  and  $[Fe\ II]$  lines. This explains why Davidson et al. (2001) found that their shape for the Homunculus derived from spectra was too small and skinny compared to images.

The inner  $[Fe\ II]$  layer and the double-shell structure may also hold clues for understanding polarization studies of the Homunculus. While dust in the outer  $H_2$  skin traces the main scattering layer seen in visual images, dust associated with the inner  $[Fe\ II]$  zone may contribute significantly to the observed polarization. If the outer layer contains predominantly large grains that behave like blackbodies at thermal-IR wavelengths, and the inner  $[Fe\ II]$  layer contains smaller grains with higher temperatures (as observed) that are seen through holes in the clumpy  $H_2$  skin, it may go a long way toward explaining the apparent contradictions in grain properties inferred independently from thermal-IR emission and visual to near-IR polarization (Walsh & Ageorges 2000; Schulte-Ladbeck et al. 1999; Smith et al. 2003b).

The  $[Fe\ II]$  layer is thicker and more irregular than the  $H_2$  shell, partially filling the interior of the lobes, especially evident in Figure 3. Its origin and relationship to the more massive  $H_2$  shell are not clear. On one hand, the observed double-shell structure resembles a classic two-shock structure of a wind plowing into an ambient medium. In this interpretation, the  $[Fe\ II]$  shell might represent emission from cooling stellar wind material that has passed through a reverse shock. The actual shock velocity could be quite low (less than  $100\text{ km s}^{-1}$ ), since the Homunculus expansion speed at high latitudes is not much different than the posteruption stellar wind speed (Smith et al. 2003a). On the other hand, the  $[Fe\ II]$  (and warm dust) layer may simply be a photodissociation region, where the radiation field from the central star is still too strong to allow  $H_2$  to exist. Dust in this region attenuates UV light, eventually allowing  $H_2$  to survive at larger radii (see, e.g., Ferland et al. 2005). An almost identical double-shell structure of  $H_2$  and  $[Fe\ II]$  also exists in the famous planetary nebula M2-9 (Hora & Latter 1994; Smith et al. 2005).

<sup>3</sup> The Little Homunculus appears “stretched” horizontally when compared to the larger Homunculus in  $[Fe\ II]$  emission in Figs. 2 and 3. This is because it is younger and thus follows a different Hubble law than the larger Homunculus (Smith 2005; Ishibashi et al. 2003).

At all five slit positions, the  $[Fe\ II]$  emission from the Little Homunculus is much brighter in the blueshifted (SE) lobe, while the  $[Fe\ II]$  from the larger Homunculus is always brighter in the redshifted (NW) lobe. Previously, this had been interpreted as attenuation of light from the NW lobe of the Little Homunculus as it passed through dust in the equator (Smith 2005), while the brightness asymmetry in the larger lobes was caused by the thick polar caps and thinner side walls of the nebula (Davidson et al. 2001; Hillier & Allen 1992). Together, these two explanations have a hint of inconsistency. A more plausible conjecture might be that the redshifted Little Homunculus lobe has a lower density and is therefore optically thinner in the Balmer continuum, allowing more UV to leak through to illuminate the larger polar lobe. A higher density in the SE polar lobe of the Little Homunculus would explain why it is brighter in the near-IR and may help explain the variable extended radio continuum and predominantly blueshifted radio recombination lines (Duncan & White 2003; Duncan et al. 1995). In any case, the spatial extent of the Little Homunculus (Smith 2005) matches the extent of variable radio continuum emission (Duncan & White 2003), so it would appear that the radio outbursts of  $\eta$  Car during the 5.5 yr cycle are due to the Little Homunculus absorbing all the Lyman continuum radiation that escapes from a variable central source.

Some faint  $[Fe\ II]$  emission from the equatorial skirt is present as well in panels *b* and *c* of Figures 2 and 3, as had been seen previously in  $[Fe\ II]$ ,  $[Ni\ II]$ ,  $[Ca\ II]$ , and  $He\ I\ \lambda 10830$  (Zethson et al. 1999; Davidson et al. 2001; Smith 2002a; Hartman et al. 2004). The reader should be cautioned that the curved  $[Fe\ II]$  emission feature extending from the center to the lower right in each panel of Figure 2 is not intrinsic emission from gas in the Homunculus; it is a narrow emission line from the Weigelt knots near the star that is reflected and redshifted by expanding dust in the SE polar lobe (see Smith 2002a; Davidson et al. 2001).

### 3.2. The Thin Outer $H_2$ Shell

While bright  $[Fe\ II]$  emission is seen in all nebulae around luminous blue variables (Smith 2002b),  $\eta$  Car is the only one where  $H_2$  emission has been detected. This unique emission feature in the Homunculus turns out to be extremely valuable in deducing the shape and other physical properties of the Homunculus, as detailed in the rest of this paper. This is because the  $H_2$  emission traces the cool and dense outer skin of the Homunculus, which thermal-IR observations indicate contains the majority of the nebula’s mass and kinetic energy (Smith et al. 2003b).

Seen at the high spectral resolution provided by the Phoenix spectrograph on Gemini South, the outer  $H_2$  skin is remarkably thin and uniform. The thickness of the  $H_2$  shell ( $\Delta R$ ) is typically 300–600 AU  $[(0.5-1) \times 10^{16}\text{ cm}]$ , or roughly 2%–3% of the polar radius ( $R$ ). This gives us an important clue to the short duration of the most important mass loss during the Great Eruption. In previous studies, I have commented that the thickness of the lobes compared to their largest radius ( $\Delta R/R$ ) is about  $1''/8''$ , which is the same as the duration of the bright phase of the Great Eruption compared to the time elapsed since then:  $\Delta t/t = 20\text{ yr}/160\text{ yr}$  (Smith et al. 1998, 2003b; Smith 2002a). However, now we see that this estimate corresponds to both the inner and outer portions of the double shell structure, with only a small fraction of the mass ( $\lesssim 10\%$ ) found in the thicker, warmer inner shell. The very thin outer shell, where 90% of the mass resides, would seem to imply that  $\Delta t/t$  is only a few percent, so that the duration of the dominant mass ejection phase was  $\lesssim 5\text{ yr}$ . This is supported by the small age dispersion derived from high-precision proper motion measurements with *HST* (e.g., Morse et al. 2001). This, in turn, would imply a *huge* instantaneous mass-loss rate

during the peak of the eruption of about  $2\text{--}5 M_{\odot} \text{yr}^{-1}$ . This may be higher than the limit for a super-Eddington continuum-driven wind (Owocki et al. 2004; Shaviv 2000). Such a short duration for the eruption and the corresponding high ratio of mechanical to radiative energy may point instead to a mechanism more like a hydrodynamic explosion originating deep within the star (e.g., Arnett et al. 2005; Young 2005). However, the very thin  $\text{H}_2$  skin also requires a very small velocity dispersion at each latitude during the original ejection, which is not a property that one usually associates with an explosion. A caveat, of course, is that even though the Homunculus is seen as a Hubble flow today, we cannot be certain that  $\Delta R/R$  exactly traces  $\Delta t/t$ , since thermal collapse of the shell or “pileup” in the ejecta may have occurred during or shortly after the eruption.<sup>4</sup> No observations currently exist with which one can reliably rule out either possibility, so both wind and explosion models are worth exploring theoretically.

In any case, the outer  $\text{H}_2$  skin is remarkably thin at the present epoch, thinner than had been recognized in previous near-IR spectroscopy or thermal-IR imaging (Smith 2002a; Smith et al. 2003b). This narrow outermost layer gives rise to a sharp absorption feature at  $-513 \text{ km s}^{-1}$ , where it crosses our line of sight to the central star, seen in  $\text{H}_2$  as well as several low-ionization metals like  $\text{Ti II}$  and  $\text{Fe I}$  in UV spectra of  $\eta$  Car (Gull et al. 2005; Nielsen et al. 2005). Instead of tracing just one sight line, long-slit near-IR spectra have the advantage of showing emission patterns from the full Homunculus. Comparing the UV absorption profiles of Gull et al. (2005) to the spectra in Figure 2, it is clear that the  $-513 \text{ km s}^{-1}$  component is from the outer  $\text{H}_2$  skin, the  $-146 \text{ km s}^{-1}$  component arises in the “Little Homunculus” (as noted already by Smith 2002a and Smith 2005), and the several intermediate-velocity components seen in low-ionization metals correspond to the thick, lumpy  $[\text{Fe II}]$ -emitting layer seen in the near-IR (note that the  $-513$  and  $-146 \text{ km s}^{-1}$  absorption components are identified by small white dots on the spectrum with the slit passing through the star in Figs. 2 and 3).

In the discussion in following sections, it will ease matters if it is fair to assume that the  $\text{H}_2$  layer can be approximated as a thin skin of uniform density and constant thickness. The  $\text{H}_2$  skin obviously has some clumping and some minor brightness variations, but overall the shell has a remarkably constant thickness and brightness, certainly within  $\pm 50\%$ . One apparent exception to the large-scale symmetry is in the portions of the walls of the polar lobes that run tangent to our line of sight, projected near the position of the star. These portions appear much fainter in Figure 2 than the corresponding parts of the lobes at the same latitudes ( $0^\circ\text{--}40^\circ$ ), which are nearly in the plane of the sky and are seen perpendicular to the dispersion direction. These differences give the impression of strong point symmetry in the brightness distribution at low latitudes in the Homunculus. However, it is not certain that this effect is real. The problem is that the fainter portions are narrow features stretching along the dispersion direction and coincide spatially with very bright reflected continuum emission that has been subtracted. It is quite possible that some  $\text{H}_2$  emission was subtracted out when attempting to fit the continuum at these positions. These regions may also suffer considerable internal extinction as we look through the limb of the outer dust shell. On the other hand, if these differences mark a real deficit of material, then the possible departures from a uniform-density model discussed here are in the sense that there will be additional missing material at low latitudes in the side

walls of the polar lobes, as compared to the assumption of a uniform skin. This would only reinforce the general conclusion that most of the mass is at high latitudes (see § 5).

#### 4. DEFINITIVE SHAPE OF THE POLAR LOBES

Since near-IR  $\text{H}_2$  emission traces the outer dust shell with most of the mass in the Homunculus and the primary dust scattering layer that dominates continuum images of the reflection nebula (e.g., Davidson & Ruiz 1975), it is our most valuable diagnostic of the true shape of the Homunculus.<sup>5</sup> The slit position passing through the central star is best for this purpose, as it is oriented along the symmetry axis of the nebula at P.A.  $\simeq 310^\circ$ .

The age of the Homunculus is  $\sim 160$  yr based on proper motion measurements and on the most dramatic change in brightness during the Great Eruption (Currie et al. 1996; Smith & Gehrz 1998; Morse et al. 2001; Frew 2004), and the entire outflow is essentially a Hubble flow. Therefore, the observed Doppler shift in  $\text{km s}^{-1}$  ( $V_R$ ) translates directly to distance from the plane of the sky as  $D_R = 33.5 V_R$ , measured in AU. Similarly, for a given distance from Earth, the pixel scale in arcseconds can be converted to a physical distance in the plane of the sky in order to create a model shape with the correct physical proportion. Assuming axial symmetry then yields an independent estimate of the distance to  $\eta$  Car, and the orientation of the homunculosity (see also Davidson et al. 2001).

##### 4.1. A Symmetric Model Shape

Figure 4 shows the measured  $\text{H}_2$  emission shape for a cross section through the symmetry axis of the Homunculus (with the slit centered on the star). The relative scale of the spatial and velocity axes was adjusted to yield a model shape with the greatest degree of axial symmetry, and then rotated so that the polar axis is vertical in Figure 4 (Figs. 3f–3h were created the same way). The distance and inclination angle adopted to make Figure 4 are  $D = 2350 \pm 50 \text{ pc}$  and  $i = 41.0^\circ \pm 0.5^\circ$ , respectively. The inclination angle  $i$  given here corresponds to the tilt of the polar axis out of the line of sight. It is the same quantity as the inclination defined for binary system orbits, so that the polar axis is tilted from the plane of the sky by  $49^\circ$ . The uncertainty is dominated by real deviations from axial symmetry in the Homunculus, which are of order 2%–3% of the radius. This distance estimate is larger than previous estimates using the same technique (Smith 2002a; Davidson et al. 2001; Allen & Hillier 1993), but the various studies agree to within the uncertainty. The distance derived here, however, is the first to use high-resolution data for the outer  $\text{H}_2$  shell that is actually seen in images, instead of the interior  $[\text{Fe II}]$  and  $[\text{Ni II}]$  emitting layer.

The best-fitting idealized symmetric model for the shape of the polar lobes is plotted over the data in Figure 4. This curve provides a direct measure of the size (radial separation from the star in AU) of the Homunculus as a function of latitude, which is listed in Table 1. This is a definitive measure of the true 3D shape of the nebula; it supersedes previous efforts largely because Doppler shifts of the narrow molecular hydrogen line constitute such a powerful and unique tracer of the outer massive shell of the Homunculus. Earlier studies using optical  $[\text{Fe II}]$  and  $[\text{Ni II}]$  were not measuring the outer shell at all but instead measured the inner shell, which has an entirely different shape. The word “definitive” in this context is not hyperbole, because one cannot

<sup>4</sup> It is unlikely, however, that the thin shell was swept up by the posteruption stellar wind long after the eruption, since the characteristic Rayleigh-Taylor-like structures that we might expect in that scenario are absent in the  $\text{H}_2$  shell.

<sup>5</sup> In hindsight,  $\text{Ca II H}$  and  $\text{K}$  absorption is also a useful diagnostic, as it seems to be located at slightly larger radii than the  $[\text{Fe II}]$  shell (Davidson et al. 2001; Smith 2002a). However, it is seen in absorption, tracing only the near side of each lobe.

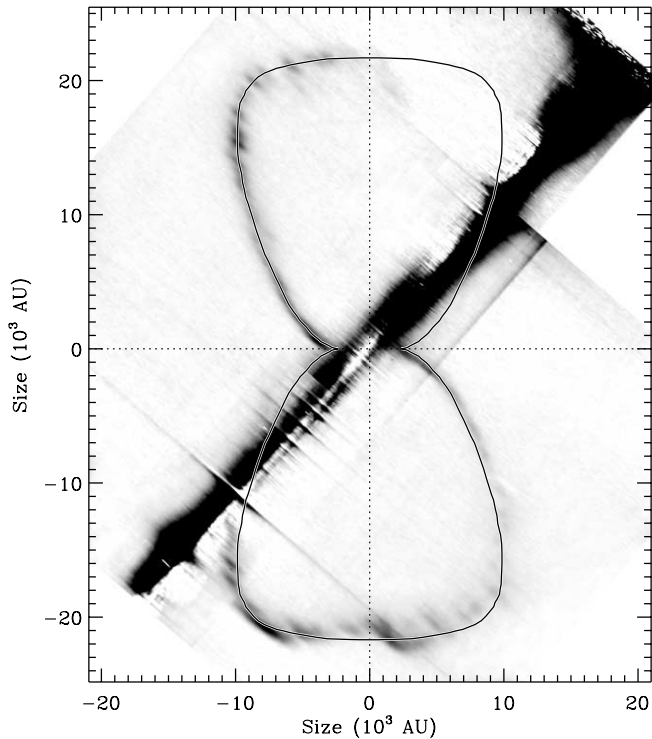


FIG. 4.—Model shape from Table 1 is plotted over  $H_2 \lambda 21218$  emission from the Homunculus. The gray-scale  $H_2$  emission is based on the same data as in Fig. 2c, but the velocity scale was converted to AU by the factor appropriate for an age of 160 yr and a distance of 2.35 kpc (as in Figs. 3f, 3g, and 3h). This yielded an “image” of a slice through the polar lobes and the star along our line of sight. The resulting image was then rotated by the apparent inclination angle of the system of  $41^\circ$  so that the polar axis appears vertical here. The unpleasant dark feature running diagonally through the image is residual continuum emission after subtraction of the bright central star, which was saturated.

do much better with observational data, uncertainties in the derived model shape are dominated by the inherent corrugations in polar lobe surfaces, which are, in turn, comparable to the thickness of the shell. Hopefully, the model shape in Figure 4 and Table 1 will be used to constrain future theoretical investigations of the formation of bipolar nebulae in general and the Homunculus in particular.

#### 4.2. Some Details: Departures from Axial Symmetry

Of course, the Homunculus lobes are not *perfectly* symmetric. Departures from axial symmetry are most apparent in the near side of the SE lobe, which appears somewhat scrunched or “snub nosed” overall and has a few large dents at some slit positions, especially at the corners and right at the polar axis. These features have been mentioned before as they are apparent in images (e.g., Morse et al. 1998). This is only obvious in the SE lobe; by contrast, the NW lobe shape obeys axial symmetry to a higher degree, showing only a few minor corrugations.

Overall, the  $H_2$  shell appears smoother in the side walls than in the polar caps. The polar regions of the lobes show several clumps or cells in the  $H_2$  spectra, as well as in high-resolution *HST* images (Morse et al. 1998). These correspond to minor wiggles or corrugations in the shape of the nebula, but these deviations from a smooth shape in the radial direction are smaller than sizes of cells in images. In other words, these are not 3D “clumps” in the normal sense, but rather, fractal divisions of the outer shell’s surface. They are more like irregular plates in the thin shell, which bring to mind analogies with rapid cooling and thermal instabilities or convection cells. These analogies may

TABLE 1  
HOMUNCULUS MODEL SHAPE

Latitude (deg)	Radius (AU)	Expansion Speed ( $\text{km s}^{-1}$ )	X Size (AU)	Y Size (AU)
0.0.....	2100	62	2100	0.0
2.0.....	2349	70	2347	82
4.0.....	2997	89	2990	209
8.6.....	3709	111	3668	555
13.9.....	4365	130	4237	1049
18.7.....	4961	148	4698	1594
21.9.....	5608	167	5202	2097
25.3.....	6276	187	5675	2681
28.6.....	6858	205	6021	3284
31.6.....	7422	222	6323	3887
34.2.....	7999	239	6613	4501
36.5.....	8654	258	6957	5149
38.7.....	9259	276	7225	5790
40.7.....	9935	297	7530	6481
42.1.....	10545	315	7824	7071
43.9.....	11200	334	8075	7761
45.5.....	11880	355	8327	8474
46.8.....	12487	373	8551	9100
48.3.....	13156	393	8756	9820
49.4.....	13823	413	8990	10500
50.5.....	14472	432	9210	11164
51.6.....	15044	449	9336	11798
52.6.....	15622	466	9481	12417
53.8.....	16275	486	9624	13126
54.7.....	16886	504	9753	13786
55.8.....	17503	523	9837	14478
56.9.....	18097	540	9869	15169
58.1.....	18716	559	9883	15895
59.1.....	19255	575	9878	16528
60.2.....	19779	591	9819	17170
61.4.....	20374	608	9739	17896
62.9.....	20898	624	9526	18601
64.3.....	21323	637	9249	19213
65.9.....	21641	646	8850	19749
67.7.....	21906	654	8327	20262
69.5.....	22014	657	7710	20621
71.3.....	22012	657	7060	20850
73.1.....	22001	657	6400	21050
74.9.....	21967	656	5740	21204
76.6.....	21932	655	5100	21332
78.3.....	21892	654	4450	21435
79.9.....	21873	653	3800	21540
81.8.....	21833	652	3100	21613
83.8.....	21774	650	2370	21645
85.6.....	21730	649	1660	21667
87.3.....	21711	648	1005	21688
89.1.....	21690	648	335	21688

NOTES.—See Fig. 6. The last two columns are the Cartesian sizes of each point in the model shape in AU.

be appropriate during the optically thick, rapidly cooling phase shortly after the material was ejected. The bright  $H_2$  features, presumably tracing the densest material, correspond to bright features in optical images, rather than dark lanes.

The maximum radial expansion speed does not occur at the pole, but at latitudes around  $65^\circ$ – $70^\circ$  (Fig. 5a). This gives rise to a hint of a trapezoidal shape to the lobes of the Homunculus. This trapezoidal shape is even more distinct in the polar lobes of the LH, suggesting a common physical mechanism at work. One possibility is that this results from extra ram pressure inside the corners of the lobes, arising from the deflection of the

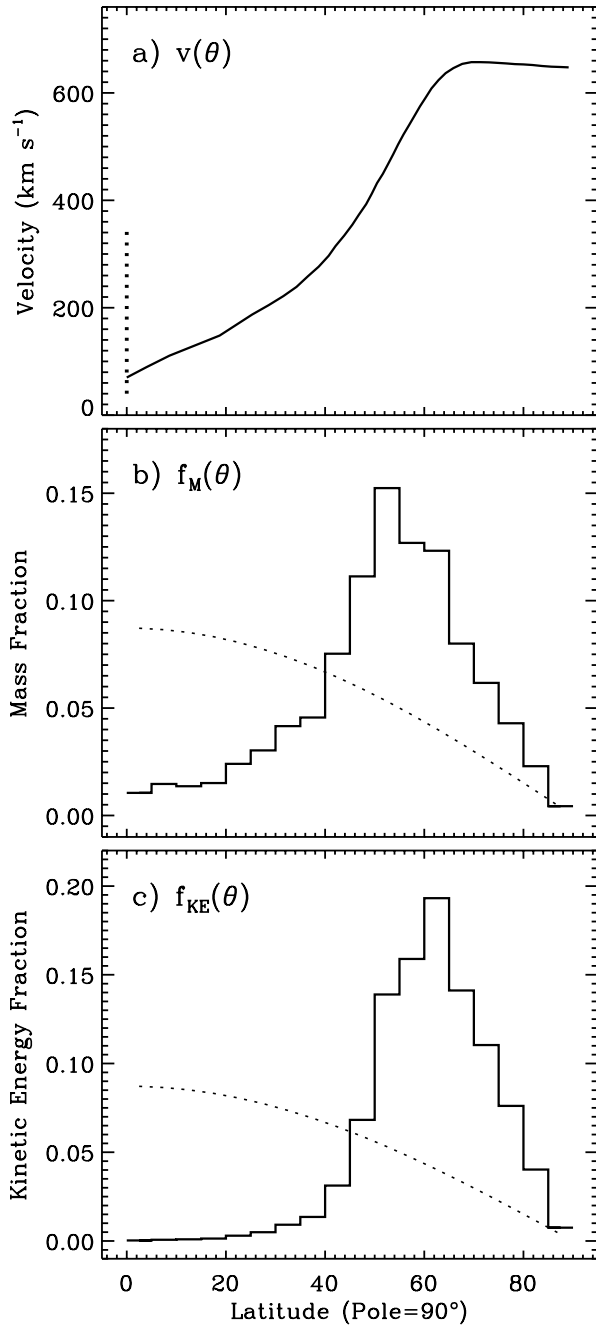


FIG. 5.—Physical properties of the Great Eruption as a function of latitude, as traced by H<sub>2</sub> emission from the polar lobes. The ejection velocity (a) is calculated from the shape in Fig. 4 and Table 1, with an age of 160 yr. The dashed vertical line at  $\theta = 0^\circ$  just accounts for the presence of the equatorial skirt inferred from images, since it does not appear in H<sub>2</sub> emission. (b) Fraction of the total mass ( $f_M$ ) as a function of latitude in  $5^\circ$  bins, assuming constant shell density and thickness across the surface area of the Homunculus. (c) The fraction of the total kinetic energy in each  $5^\circ$  latitude bin, from the corresponding mass fraction and velocity above. The dotted curves in panels b and c correspond to the same quantities for a uniform spherical shell.

posteruption wind that strikes the inner side walls of the polar lobes at an oblique angle. Such effects are present in simulations of bipolar wind-blown bubbles (e.g., Cunningham et al. 2005; Frank et al. 1998). This extra ram pressure would not be related to the opening angle of the shock cone in a binary system, since during the eruption it is likely that the shock cone was collapsed onto the secondary star.

## 5. THE GREAT ERUPTION AS A FUNCTION OF LATITUDE

The Homunculus bears the imprint of the Great Eruption's mass loss as a function of latitude. Therefore, the shape and structure of the H<sub>2</sub> emission in high-resolution spectra provide important insight to the physics of the outburst, to the extent that H<sub>2</sub> is a good tracer of the mass.

Figure 5 shows the latitude dependence of velocity, mass loss, and mechanical energy in the Homunculus, based on H<sub>2</sub> emission. The velocity distribution follows directly from the shape of the nebula, since it is a Hubble flow. However, calculating these distributions of mass and kinetic energy requires a few assumptions. As a first approximation, the thin outer H<sub>2</sub> shell of the Homunculus is taken to be of uniform density with a constant width. The apparent width in Phoenix spectra is very nearly constant, with variations typically less than a factor of 2. Note that the thicker appearance of the H<sub>2</sub> shell at slit offset positions NE2 and SW2 (see Fig. 1) is somewhat misleading, since these slit positions slice through the lobes at an oblique angle to their surfaces. If this assumption applies, then the mass in various parts of the shell is simply proportional to its geometric surface area at each latitude. While the nebula is obviously not perfectly uniform, we see below that the important characteristics of the latitudinal distribution in the nebula are not compromised by these minor effects.

To calculate various quantities as functions of latitude, the outer shell was approximated as a series of adjacent loops or tori centered on the polar axis of the nebula (see Fig. 6). The mass for each representative latitudinal loop is given by  $2m_H n_H (\pi r^2) (2\pi R_H)$ , where  $R_H = R_H(\theta)$  is the horizontal radius of each torus measured from the polar axis (parallel to the equator), and  $2r$  is the thickness of the torus, roughly equal to the overall shell thickness of  $\sim 600$  AU (the extra factor of 2 accounts for the mass in both polar lobes). Following the assumption of constant shell thickness and uniform density, however, the fraction of the total mass at each latitude  $f_M(\theta) = M(\theta)/\Sigma M(\theta)$  is simply proportional to  $R_H$ . This quantity is plotted in Figure 5b and avoids the uncertainty in the absolute physical density, shell thickness (as long as it is constant), and total mass. The fraction of the total kinetic energy at each latitude  $f_{KE}(\theta) = M(\theta)v(\theta)^2/\Sigma[M(\theta)v(\theta)^2]$  in Figure 5c is calculated for each torus from its value of  $f_M(\theta)$  and its radial expansion speed. These rings were regularly spaced along the surface of the nebula (Fig. 6) but not spaced regularly in latitude. Therefore, before plotting in Figure 5, the values for  $f_M(\theta)$  and  $f_{KE}(\theta)$  were rebinned in latitude intervals of  $5^\circ$ .

Figure 5b indicates that most mass lost during the Great Eruption was aimed to high latitudes.<sup>6</sup> Only 25% of the total Homunculus mass was ejected at  $0^\circ < \theta < 45^\circ$ , with the remaining 75% ejected between  $45^\circ$  and the pole. The latitudinal distribution of the ejecta's kinetic energy is even more extreme, with almost all the mechanical energy ( $\sim 94\%$ ) escaping between  $45^\circ$  and the pole. The efficiency of imparting mechanical energy to the ejecta seems to peak at latitudes around  $60^\circ$ – $65^\circ$ , while the peak mass loss occurs around  $50^\circ$ – $60^\circ$ .

For comparison, the latitudinal distribution of mass and kinetic energy for a uniform spherical shell is shown by the dotted

<sup>6</sup> A deficit of mass at low latitudes raises interesting questions about the history of light escaping from the Homunculus as the ejecta expanded and thinned in the decades after the Great Eruption. For example, Frew (2004) notes that the polar lobes of the Homunculus were not seen until the 1940's (Gaviola 1950), while early visual observers noted the appearance of "nubeculi" that are associated with equatorial features (Innes 1914, 1915; Voute 1925, van den Bos 1928; see also Smith & Gehrz 1998).

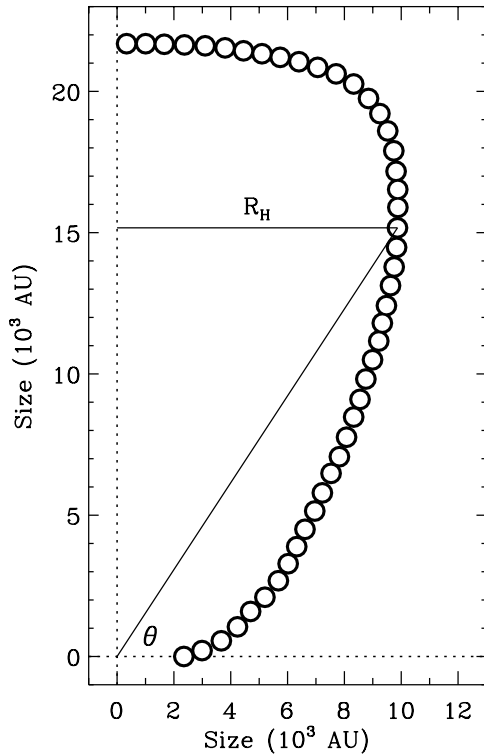


FIG. 6.—Subdivision of a uniform thin shell into a series of regularly spaced tori matching the model shape of the Homunculus, each with radius  $R_H$  from the polar axis. Each torus has the same cross-sectional area, but each takes up a different fraction of the surface area of the Homunculus, proportional to  $R_H$ . This model was used to calculate the latitude dependence of mass and kinetic energy in Fig. 5. This sort of model accounts in a crude way for an effective filling factor due to clumps in the  $H_2$  skin.

curves in Figure 5, while Figure 7 shows the mass and kinetic energy per solid angle (so that a spherical shell is a horizontal line). The differences between a spherical shell and the Homunculus are striking. This latitudinal behavior strongly refutes the idea that a bipolar nebula like the Homunculus was caused by an otherwise spherical explosion or wind that is simply pinched by a preexisting circumstellar torus, because in that case we would expect to see more mass at low latitudes (see also Dwarkadas & Balick 1998 and Soker 2001). Likewise, the mass loss during the Great Eruption could not have been redirected toward the poles by deflection from its companion star, because the amount of kinetic energy in the polar ejecta is greater than the binding energy of the current putative binary system and more than 3 orders of magnitude greater than the available energy in the companion's wind during the eruption.

Instead, the concentration of mass at high latitudes suggests that the original explosion itself directed the mass and momentum toward the poles. An alternative way to express the same result is that perhaps much of the mass that would have been ejected at  $0^\circ$ – $40^\circ$  failed to reach escape velocities and fell back onto the star. In any case, having the majority of the mass—a significant fraction of the total mass of the star—lost at polar latitudes will effect the star's angular momentum evolution. A polar explosion will tend to take away less than its share of angular momentum, leaving the postoutburst star with higher angular momentum per unit mass. This is related to its currently observed bipolar stellar wind (Smith et al. 2003a). In addition, after ejecting its own massive luminous blue variable (LBV) nebula, there is evidence that AG Carinae is also left as a rapid rotator (Groh et al. 2006).

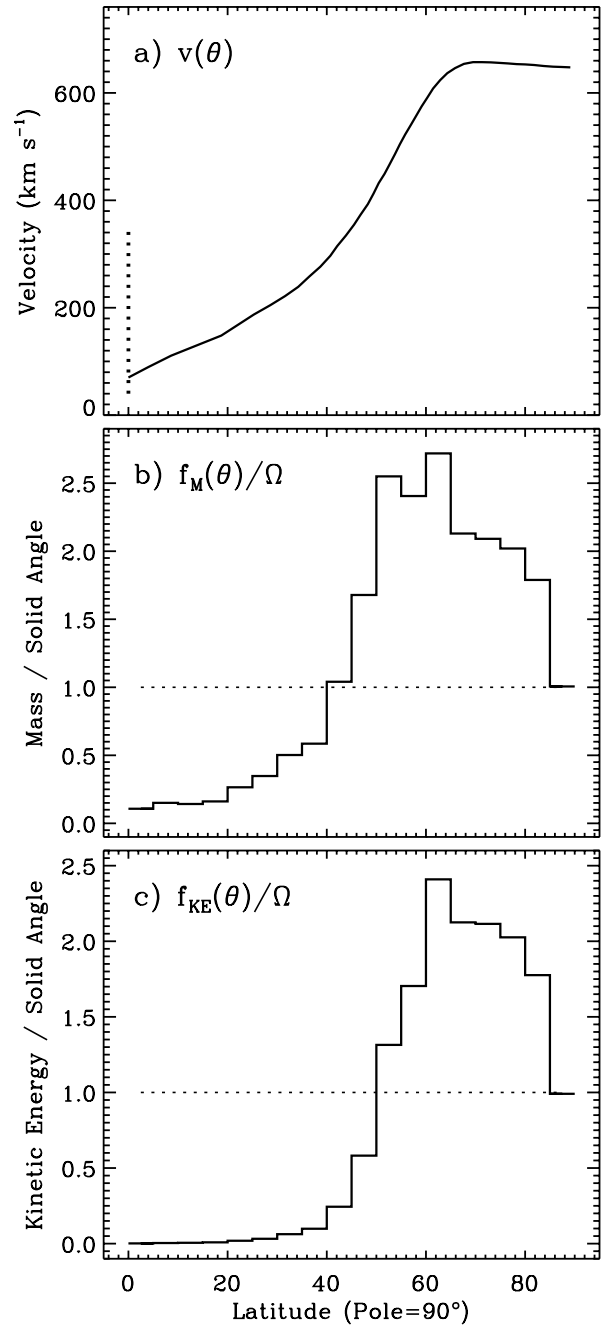


FIG. 7.—Same as Fig. 5, but showing the relative mass and kinetic energy fractions per solid angle, normalized to the value at the pole. In these plots, a spherically symmetric shell has the same mass and kinetic energy per solid angle at all latitudes.

Ultimately, without a circumstellar torus or deflection by a companion, the bipolar shape must come from rapid rotation of the primary star; in that view the role of a companion star is relegated to helping to spin up the primary star through tidal friction during repeated periastron passes (e.g., Smith et al. 2003a). If the mass loss is driven by radiation, then gravity darkening on a rapidly rotating star will tend to drive most of the mass flux toward high latitudes (e.g., Owocki et al. 1996, 1998; Owocki & Gayley 1997; Owocki 2003), providing a possible explanation for the polar mass concentration. However, it remains to be seen if even a super-Eddington continuum-driven wind can fuel the required mass loss (Owocki et al. 2004).

The latitudinal mass distribution has some interesting connections with other famous bipolar nebulae, especially the circumstellar nebula around SN 1987A. Both  $\eta$  Car and SN 1987A have nebulae with equatorial and bipolar mass loss, but the two polar rings around SN 1987A are particularly vexing. In the Homunculus of  $\eta$  Car, we see that most of the mass outflow was concentrated toward intermediate latitudes around  $65^\circ$ – $70^\circ$ . One can imagine that if the mechanism that produced this mass concentration were pushed to some extreme limit, it might produce a pair of rings as it flowed out from the star. While energy arguments rule out bipolar shaping by a companion star in an eccentric 5.5 yr orbit that survives as the putative binary system seen in  $\eta$  Car today (see above), a more exotic model in which the 1843 Great Eruption involved the merger of a tight binary system is admittedly more difficult to reject. In fact, a recent theoretical study of a merger scenario for the progenitor of SN 1987A found that most of the mass loss is directed toward mid-latitudes, with a significant deficit of mass loss near the equator (Morris & Podsiadlowski 2005). On the other hand, if one wishes to explain  $\eta$  Car's Great Eruption as a merger of two massive stars, then it is a mystery why the similar eruption of P Cygni in 1600 AD (see Humphreys et al. 1999) ejected a spherical shell (Smith & Hartigan 2006) and apparently did not leave that star as a rapid rotator.

Finally, an important caveat is needed. The notorious equatorial skirt of  $\eta$  Carinae (discussed in § 7) is not detected in near-IR  $H_2$  emission, presumably because molecules simply cannot survive or never formed there. This equatorial spray of ejecta seen in images is quite extensive and reaches large radii from the star, comparable to some parts of the polar lobes. Thus, one should expect that the true velocity, mass, and energy distributions in Figure 5 would be modified with a spike at  $\theta = 0^\circ$ . The magnitude of this equatorial spike in the mass distribution is not known. Judging by the general absence of these equatorial features in thermal-IR images (Smith et al. 2003b), however, the skirt likely contains less than  $\sim 0.5 M_\odot$ .

## 6. MASS AND DENSITY IN THE $H_2$ SKIN

A crude estimate of the expected mass density in the  $H_2$  shell can be made from the total mass of the Homunculus and the volume occupied by the thin  $H_2$  skin. The  $H_2$  skin corresponds to the cool 140 K dust component that occupies the outer shell seen in thermal-IR images, which Smith et al. (2003b) estimate to contain at least  $11 M_\odot$ . This  $11 M_\odot$  contains about 90% of the total mass in the Homunculus, but its actual value depends on the highly uncertain gas : dust mass ratio, assumed to be 100. As noted by Smith et al. (2003b), this is most likely a lower limit to the mass, since the ejecta of  $\eta$  Car are depleted of important grain constituents like C and O, and much of the Fe is evidently in the gas phase, as reinforced by the spectra presented in this paper. Therefore, the density derived below is also a lower limit. The total volume of the model  $H_2$  skin in Figure 6 is  $V_{H_2} = 4.6 \times 10^{51} (r/300 \text{ AU})^2 \text{ cm}^3$ . Thus, the equivalent pure atomic hydrogen density in the  $H_2$  skin is given by

$$n_H > \frac{11 M_\odot}{m_H V_{H_2}} \simeq 3 \times 10^6 \text{ cm}^{-3},$$

where  $m_H$  is the proton mass and  $2r = 600 \text{ AU}$  is the assumed thickness of the  $H_2$  skin. Two points need to be stressed, (1)  $n_H > 3 \times 10^6 \text{ cm}^{-3}$  is a lower limit because the total mass estimate is a lower limit (Smith et al. 2003b) and because parts of the shell are thinner than adopted here, and (2) this is an *average* density, so densities above  $10^7 \text{ cm}^{-3}$  may be present in clumps, even if the total mass estimate is accurate.

The assumption of constant average density throughout the  $H_2$  skin may be optimistic, of course, but given the very thin side walls of the Homunculus lobes, the latitudinal mass trend in Figure 7 could only be erased (flattened) if the density were of order  $10^8 \text{ cm}^{-3}$  or more. Corresponding column densities would be  $N_{H_2} \simeq 10^{24} \text{ cm}^{-2}$ , which would contradict the fact that the side walls of the polar lobes are more optically thin than the caps (e.g., Davidson et al. 2001; Allen & Hillier 1993). Such high column densities would also contradict the much lower value of  $N_{H_2} \simeq 1.5 \times 10^{23} \text{ cm}^{-2}$  from scattered hard X-rays in the Homunculus (Corcoran et al. 2004).

Similar values of  $n_H \simeq 10^7 \text{ cm}^{-3}$  have been derived by Gull et al. (2005) from UV absorption along our sight line to the star in the lowest ionization species at a radial velocity of  $-513 \text{ km s}^{-1}$ . This rough agreement with the density value quoted here gives independent confirmation of the very high mass estimate for the Homunculus of more than  $10 M_\odot$  (Smith et al. 2003b). In fact, the volume of the  $H_2$  shell derived from Phoenix spectra and the higher density derived independently by Gull et al. would favor an even higher mass for the Homunculus of perhaps  $\sim 20 M_\odot$ .

## 7. CLUES TO THE NATURE OF THE COMPLEX CORE AND THE BIZARRE EQUATORIAL EJECTA

While the shape, orientation, and density structure of the polar lobes seem understandable in the framework of the double-shell structure discussed here, the morphology of the messy equatorial skirt is still perplexing. However, the new Phoenix spectra from Gemini South shed some light on this mystery.

One important clue is that the material in the extended equatorial skirt shows no detectable infrared  $H_2$  emission, despite residing at large radii where it should be shielded by dense dusty structures in the core region. The features in the equatorial skirt, while prominent in reflected light at visual wavelengths (Morse et al. 1998; Duschl et al. 1995), have weak emission in the thermal-IR (Smith et al. 2003b). These facts suggest that the equatorial disk has much lower density than the walls of the lobes, and so dust and molecule formation was less efficient there in the decades after the Great Eruption. In fact, some equatorial features seem to be optical illusions (Davidson et al. 2001). Thus, the equatorial skirt contains only a small fraction of the total mass in the Homunculus; probably  $\lesssim 0.5 M_\odot$ , as noted above.

The spatial and kinematic structure in high-resolution spectra of  $H_2$  give the first clear picture of the shape and structure of the Homunculus at low latitudes near the equator where the two polar lobes meet. This region is hidden in images and visual-wavelength spectra due to obscuration from the foreground lobe, and the [Fe II] emission there is very confusing due to the Little Homunculus (Ishibashi et al. 2003; Smith 2005) and structures near the star like the so-called ‘‘Weigelt knots’’ and other clumps (Weigelt et al. 1995; Davidson et al. 1997; Smith et al. 2004; Smith 2005; Chesneau et al. 2005). Thermal emission from dust traces an extremely complicated distribution of interconnected clumps, arcs, and diffuse emission seen most clearly in high-resolution images at 2–8  $\mu\text{m}$  (Chesneau et al. 2005; Smith et al. 2002, 2003b; Smith & Gehrz 2000; Rigaut & Gehring 1995). This is the warmest dust ( $T > 250 \text{ K}$ ) in the core of the Homunculus, long thought to constitute some sort of a warm torus (Hyland et al. 1979; Mitchell et al. 1983; Hackwell et al. 1986; Smith et al. 1995, 1998; Polomski et al. 1999). Two recent papers with the best IR images to date suggested two very different interpretations of these complex structures: (1) Smith et al. (2002) proposed that they mark a distorted and disrupted torus or ring where the two polar lobes of the Homunculus meet at the equator. In this view, the complex structures are a result of lower density structures

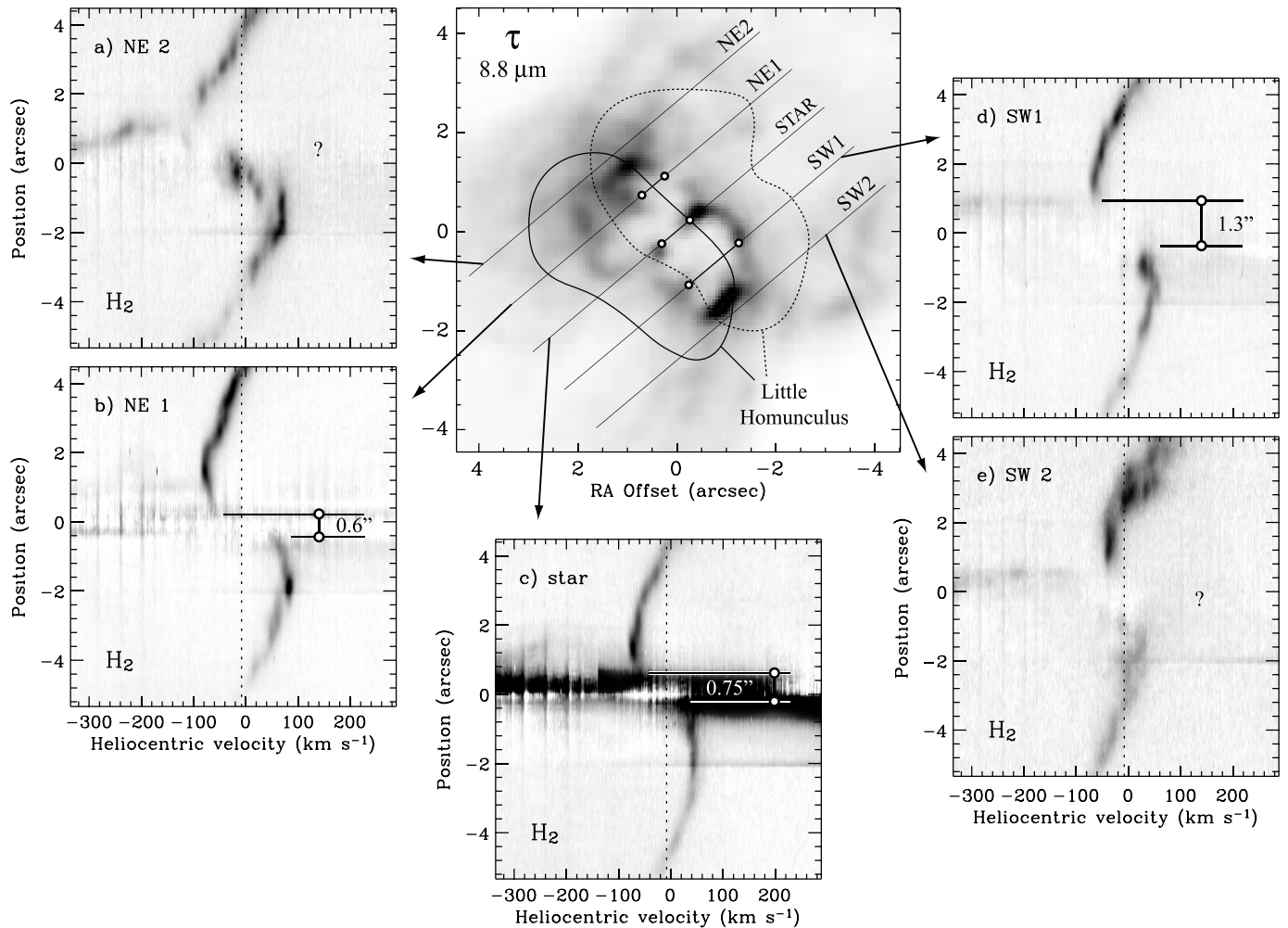


FIG. 8.— Center panel is the warm dust column density map ( $8.8 \mu\text{m}$  optical depth from Smith et al. 2003b), showing the bright dust structures near the core that have been interpreted as either a dust torus or a “Butterfly Nebula.” Panels *a–e* are the same as the  $\text{H}_2$  spectra in Figs. 2*a–2e*, but zoomed in on the central structures. The purpose of this figure is to illustrate the correspondence between spatial gaps in  $\text{H}_2$  emission in spectra and the size of the cavity in the interior of the dust torus. The NE2 and SW2 slit positions do not cut through the interior of the torus, but for NE1, the star, and SW1, the gap in  $\text{H}_2$  emission in each panel is superposed on the dust image as dots connected by a short solid line. The gaps in  $\text{H}_2$  emission match the interior of the dust torus, proving that this is an equatorial structure where the two polar lobes meet, rather than a bipolar “Butterfly Nebula.” The spatial extent of the Little Homunculus from Smith (2005) is shown as well, indicating that the dust structures do not arise in the Little Homunculus.

getting swept back by the post eruption stellar wind, and higher density clumps resisting that expansion. (2) Chesneau et al. (2005) proposed the existence of a new structure called the “Butterfly Nebula,” which was a dusty bipolar nebula different from the Little Homunculus and which had the dust reaching back toward the star along the polar axis. The new  $\text{H}_2$  spectra distinguish clearly between these two hypotheses.

Figure 8 demonstrates the correspondence between the structures seen in a high-resolution map of the warm dust column density near the star from Smith et al. (2003b) and the spatial and kinematic structure of  $\text{H}_2$  emission in spectra. Where the thin  $\text{H}_2$  walls of the Homunculus meet at the equator, they do not reach all the way in to the star but instead leave a gap in the apparent distribution of  $\text{H}_2$  along the slit. This gap is slightly different at each slit position and is noted in each spectral image. Each of these gaps is superposed on top of the IR continuum image, where we see that indeed the spatial limits of  $\text{H}_2$  emission correspond nicely to the empty interior of the so-called Butterfly Nebula or torus. The agreement between  $\text{H}_2$  in the walls of the Homunculus and the dust structures prove that this really is an equatorial torus or ring where the polar lobes meet at the equator, rather than the

separate nebular structure proposed by Chesneau et al. (2005). The toroidal interpretation also gives a more natural explanation for the deficit of IR emission within its boundaries (Chesneau et al. 2005). No kinematic evidence for the putative butterfly structure is seen in spectra, and the dust structures are not coincident with the Little Homunculus either (Fig. 8). The question then is: if these structures represent parts of an equatorial torus or ring, why does it exhibit such prominent azimuthal asymmetry (clumps, arcs, etc.), while the rest of the  $\text{H}_2$ -emitting portions of the Homunculus, by comparison, show such well-ordered axisymmetric structure?

The strange clumps and arcs in this equatorial dust structure, and the lack of similar features in the polar lobes, can be understood as follows (Smith et al. 2002). In the 160 yr since the Homunculus was ejected in the Great Eruption, it has been followed by the posteruption stellar wind. At the poles, the speed for the bulk of the post eruption wind is about  $600 \text{ km s}^{-1}$  (traced by the deepest part of the  $\text{H}\alpha$  P Cygni absorption; Smith et al. 2003a), which is almost identical to the expansion speed of the Homunculus (Fig. 5*a*). With such a small  $\Delta v$ , we expect little or no hydrodynamic influence from the wind. The equator presents a very

different story. Although the present-day stellar wind is bipolar, it appears to maintain relatively high wind speeds of  $\sim 400 \text{ km s}^{-1}$  at the equator (Smith et al. 2003a), whereas the pinched waist of the Homunculus seen in  $\text{H}_2$  has very slow velocities of only a few dozen  $\text{km s}^{-1}$ . This large value of  $\Delta v$  right at the equator should lead to Rayleigh-Taylor or nonlinear thin-shell instabilities (Vishniac 1994) in the torus where the polar lobes meet, much like any other dense ejecta shell followed by a faster wind (e.g., Garcia-Segura et al. 1996).<sup>7</sup> The Homunculus is inherently clumpy at all latitudes, perhaps even more so at the equator (ud Doula & Owocki 2002). Since the ram pressure of the incident wind depends on  $(\Delta v)^2$ , the posteruption wind is most influential at the equator. Any clumps in this ring will resist the ram pressure of the wind more than the less dense regions between them. The interclump sections of the torus would be swept back, leading to structures akin to dust pillars in  $\text{H II}$  regions. In other words, the values in the first row of Table 1 are azimuthally dependent. This is essentially a more extreme version of the Rayleigh-Taylor instabilities that are thought to have led to the early development of hot spots in the famous equatorial ring around SN 1987A (e.g., Michael et al. 2000; Sugerman et al. 2002).

In the interclump regions of the torus, where the wind pushes outward, there may be an interesting link to the unusual structures seen in  $\eta$  Car's equatorial skirt. (The equatorial skirt is the more extended disk with peculiar radial streamers or spokes that seem to point back to the star [Duschl et al. 1995; Morse et al. 1998].) In the interclump regions of the torus that are pushed to larger radii, light may more easily leak through to illuminate outer regions of the skirt (i.e., searchlights like the radial features in the Egg Nebula; Sahai et al. 1998). In some extreme cases, the stellar wind or ejecta from the Great Eruption or the 1890 eruption may even have broken through the Homunculus. Some material in the skirt is indeed seen to have kinematics consistent with ejection during the 1890 eruption (Davidson et al. 2001; Smith 2002a), and some more extended equatorial features like the NN jet and the S condensation appear to have originated in the Great Eruption (Morse et al. 2001). These searchlights or ejecta breaking through the Homunculus in the equator provide a natural explanation for the quasi-radial spokes or streamers seen in the equatorial skirt. These features in the skirt may be largely an illumination effect, while the true distribution of matter in the equatorial disk may be considerably more azimuthally symmetric than it appears.

## 8. CONCLUSIONS

New high-resolution, long-slit spectra of  $\text{H}_2$   $\lambda 21218$  and  $[\text{Fe II}]$   $\lambda 16435$  from the Phoenix spectrograph on Gemini South provide new clues to the detailed structure of the Homunculus. The main conclusions of this study are summarized as follows.

1. The relative spatio-kinematic structure of infrared  $\text{H}_2$  and  $[\text{Fe II}]$  emission gives an independent confirmation of the double-shell structure for the polar lobes of the Homunculus proposed on the basis of thermal-IR images (Smith et al. 2003b). The inner  $[\text{Fe II}]$  layer corresponds to the warmer (200 K) inner dust layer that traces only about 10% of the mass of the Homunculus,

while the outer  $\text{H}_2$  skin traces the coolest dust component (140 K) that contains the remaining 90% of the nebular mass.

2. The high-resolution spectra of  $\text{H}_2$  show for the first time how thin and surprisingly smooth the outer molecular skin of the Homunculus is. If the  $\text{H}_2$  skin's  $\Delta R/R$  traces  $\Delta t/t$  of the mass ejection, then the most important mass-loss phase during the eruption is constrained to be about 5 yr or less. The corresponding mass-loss rate is so high that the mechanical luminosity would have greatly exceeded the radiative luminosity at that time, implying that the Great Eruption was more of an explosion than a wind.

3. A lower limit to the density within the  $\text{H}_2$  layer, based on a lower limit to the mass of the Homunculus (Smith et al. 2003b) and the apparent volume of the  $\text{H}_2$  skin, is  $n_{\text{H}} \gtrsim 10^{6.5} \text{ cm}^{-3}$ .

4. Since  $\text{H}_2$  emission traces most of the mass in the Homunculus as well as the dominant dust-scattering layer seen as a reflection nebula in images,  $\text{H}_2$  spectra give the first definitive picture of the three-dimensional shape of the Homunculus, which is given in Table 1. Earlier estimates of the shape and orientation traced the inner  $[\text{Fe II}]$ -emitting layer, which has a different size and structure.

5. The model shape combined with the known age of the nebula gives a distance of  $2350 \pm 50 \text{ pc}$  to  $\eta$  Car and an inclination of  $i = 41^\circ \pm 0.5^\circ$  for the polar axis.

6. Deviations from a smooth symmetric shape are minor, generally comparable to the thickness of the lobes. The redshifted NW lobe appears more symmetric than the approaching SE lobe, which shows more prominent dents and corrugations.

7. The  $\text{H}_2$  distribution yields our first estimate of the latitudinal dependence of the velocity, mass loss, and kinetic energy of the Great Eruption. About 75% of the mass and more than 90% of the mechanical energy were released at latitudes between  $45^\circ$  and the pole.

8. This latitudinal mass distribution rules out a model in which the bipolar shape of the nebula arises from an otherwise spherical explosion being constricted by a preexisting circumstellar torus. The kinetic energy of the polar ejecta rule out a model in which the ejecta were deflected toward the poles by a companion star, because the putative companion could not have supplied the required energy. This means that the ejecta were directed toward the poles by the explosion itself. A merger event is not as easy to rule out, but is unlikely.

9. The spatio-kinematic structure of  $\text{H}_2$  emission at the pinched waist of the nebula helps explain the unusual and complex structures seen in high-resolution IR images as an equatorial torus disrupted by the posteruption wind. The radial structures in the equatorial skirt seen in visual-wavelength images are the result of either beams of light or ejecta that have broken through the inner dust torus.

I thank Verne Smith and Sybil Adams for assistance during the Gemini South observing run, and Keivan Stassun for diligently obtaining numerous dark frames with Phoenix earlier in the same observing nights. I also thank Kris Davidson and Stan Owocki for comments on the manuscript and numerous discussions. I was supported by NASA through grant HF-01166.01A from the Space Telescope Science Institute, which is operated by the Association of Universities for Research in Astronomy, Inc., under NASA contract NAS5-26555.

<sup>7</sup> The much lighter and slower shell around P Cygni is a good example of this (Smith & Hartigan 2006).

## REFERENCES

- Aitken, D. K., Smith, C. H., Moore, T. J. T., & Roche, R. F. 1995, *MNRAS*, 273, 359
- Allen, D. A., & Hillier, D. J. 1991, *Publ. Astron. Soc. Australia*, 9, 120
- . 1993, *Publ. Astron. Soc. Australia*, 10, 338
- Arnett, D., Meakin, C., & Young, P. A. 2005, in *ASP Conf. Ser. 332, The Fate of the Most Massive stars*, ed. R. M. Humphreys & K. Z. Stanek (San Francisco: ASP), 75
- Chesneau, O., et al. 2005, *A&A*, 435, 1043
- Corcoran, M. F., et al. 2004, *ApJ*, 613, 381
- Cunningham, A., Frank, A., & Hartmann, L. 2005, *ApJ*, 631, 1010
- Currie, D. G., et al. 1996, *AJ*, 112, 1115
- Davidson, K., Ebbets, D., Weigelt, G., Humphreys, R. M., Hajian, A. R., Walborn, N. R., & Rosa, M. 1995, *AJ*, 109, 1784
- Davidson, K., & Ruiz, M. T. 1975, *ApJ*, 202, 421
- Davidson, K., & Smith, N. 2000, *Nature*, 405, 532
- Davidson, K., Smith, N., Gull, T. R., Ishibashi, K., & Hillier, D. J. 2001, *AJ*, 121, 1569
- Davidson, K., et al. 1997, *AJ*, 113, 335
- Duncan, R. A., & White, S. M. 2003, *MNRAS*, 338, 425
- Duncan, R. A., White, S. M., Lim, J., Nelson, G. J., Drake, S. A., & Kundu, M. R. 1995, *ApJ*, 441, L73
- Duschl, W. J., Hofmann, K. H., Rigaut, F., & Weigelt, G. 1995, *Rev. Mex. AA Ser. Conf.*, 2, 17
- Dwarkadas, V. V., & Balick, B. 1998, *AJ*, 116, 829
- Dwarkadas, V. V., & Owocki, S. P. 2002, *ApJ*, 581, 1337
- Ferland, G. J., Abel, N., Davidson, K., & Smith, N. 2005, in *ASP Conf. Ser. 332, The Fate of the Most Massive Stars*, ed. R. M. Humphreys & K. Z. Stanek (San Francisco: ASP), 294
- Frank, A., Balick, B., & Davidson, K. 1995, *ApJ*, 441, L77
- Frank, A., Ryu, D., & Davidson, K. 1998, *ApJ*, 500, 291
- Frew, D. J. 2004, *J. Astron. Data*, 10, 6
- Garcia-Segura, G., Mac Low, M. M., & Langer, N. 1996, *A&A*, 305, 229
- Gaviola, E. 1950, *ApJ*, 111, 408
- Gonzalez, R., de Gouveia Dal Pino, E. M., Raga, A. C., & Velazquez, P. F. 2004a, *ApJ*, 600, L59
- . 2004b, *ApJ*, 616, 976
- Groh, J. H., Hillier, D. J., & Daminieli, A. 2006, *ApJ*, 638, L33
- Gull, T. R., Vieira, G., Bruhweiler, F., Nielsen, K. E., & Danks, A. 2005, *ApJ*, 620, 442
- Hackwell, J. A., Gehr, R. D., & Grasdalen, G. L. 1986, *ApJ*, 311, 380
- Hartman, H., et al. 2004, *A&A*, 419, 215
- Hillier, D. J. 1997, in *ASP Conf. Ser. 120, Luminous Blue Variables*, ed. A. Nota & H. Lamers (San Francisco: ASP), 287
- Hillier, D. J., & Allen, D. A. 1992, *A&A*, 262, 153
- Hinkle, K. H., et al. 2003, *Proc. SPIE 4834, Discoveries and Research Prospects from 6- to 10-Meter-Class Telescopes II*, ed. P. Guhathakurta (Bellingham: SPIE), 353
- Hora, J. L., & Latter, W. B. 1994, *ApJ*, 437, 281
- Humphreys, R. M., Davidson, K., & Smith, N. 1999, *PASP*, 111, 1124
- Hyland, A. R., Robinson, G., Mitchell, R. M., Thomas, J. A., & Becklin, E. E. 1979, *ApJ*, 233, 145
- Innes, R. T. A. 1914, *MNRAS*, 74, 697
- . 1915, *Observatory*, 38, 333
- Ishibashi, K., et al. 2003, *AJ*, 125, 3222
- Langer, N., Garcia-Segura, G., & MacLow, M. M. 1999, *ApJ*, 520, L49
- Matt, S., & Balick, B. 2004, *ApJ*, 615, 921
- Meaburn, J. 1999, in *ASP Conf. Ser. 179, Eta Carinae at the Millennium*, ed. J. A. Morse et al. (San Francisco: ASP), 89
- Meaburn, J., Walsh, J. R., & Wolstencroft, R. D. 1993, *A&A*, 268, 283
- Meaburn, J., Wolstencroft, R. D., & Walsh, J. R. 1987, *A&A*, 181, 333
- Michael, E., et al. 2000, *ApJ*, 542, L53
- Mitchell, R. M., Robinson, G., Hyland, A. R., & Jones, T. J. 1983, *ApJ*, 271, 133
- Morris, P. W., et al. 1999, *Nature*, 402, 502
- Morris, T., & Podsiadlowski, P. 2006, *MNRAS*, 365, 2
- Morse, J. A., Davidson, K., Bally, J., Ebbets, D., Balick, B., & Frank, A. 1998, *AJ*, 116, 2443
- Morse, J. A., Kellogg, J. R., Bally, J., Davidson, K., Balick, B., & Ebbets, D. 2001, *ApJ*, 548, L207
- Nielsen, K. E., Gull, T. R., & Vieira-Kober, G. 2005, *ApJS*, 157, 138
- Owocki, S. P. 2003, *IAU Symp. 212, A Massive Star Odyssey*, ed. K. van der Hucht, A. Herrero, & C. Esteban (San Francisco: ASP), 281
- Owocki, S. P., Cranmer, S. R., & Gayley, K. 1996, *ApJ*, 472, L115
- Owocki, S. P., & Gayley, K. G. 1997, in *ASP Conf. Ser. 120, Luminous Blue Variables*, ed. A. Nota & H. Lamers (San Francisco: ASP), 121
- Owocki, S. P., Gayley, K., & Cranmer, S. R. 1998, in *ASP Conf. Ser. 131, Boulder-Munich II: Properties of Hot, Luminous Stars*, ed. I. D. Howarth (San Francisco: ASP), 237
- Owocki, S. P., Gayley, K., & Shaviv, N. 2004, *ApJ*, 616, 525
- Polomski, E. F., Telesco, C. M., Piña, R. K., & Fisher, S. F. 1999, *AJ*, 118, 2396
- Rigaut, F., & Gehring, G. 1995, *Rev. Mex. AA Ser. Conf.*, 2, 27
- Ringlelet, A. E. 1958, *Z. Astrophys.*, 46, 276
- Sahai, R., et al. 1998, *ApJ*, 493, 301
- Schulte-Ladbeck, R., Pasquali, A., Clampin, M., Nota, A., Hillier, D. J., & Lupie, O. L. 1999, *AJ*, 118, 1320
- Shaviv, N. J. 2000, *ApJ*, 532, L137
- Smith, C. H., Aitken, D. K., Moore, T. J. T., Roche, P. F., Puetter, R. C., & Pina, R. K. 1995, *MNRAS*, 273, 354
- Smith, N. 2002a, *MNRAS*, 337, 1252
- . 2002b, *MNRAS*, 336, L22
- . 2004, *MNRAS*, 351, L15
- . 2005, *MNRAS*, 357, 1330
- Smith, N., Balick, B., & Gehr, R. D. 2005, *AJ*, 130, 853
- Smith, N., & Davidson, K. 2001, *ApJ*, 551, L101
- Smith, N., Davidson, K., Gull, T. R., Ishibashi, K., & Hillier, D. J. 2003a, *ApJ*, 586, 432
- Smith, N., & Gehr, R. D. 1998, *AJ*, 116, 823
- . 2000, *ApJ*, 529, L99
- Smith, N., Gehr, R. D., Hinz, P. M., Hoffmann, W. F., Hora, J. L., Mamajek, E. E., & Meyer, M. R. 2003b, *AJ*, 125, 1458
- Smith, N., Gehr, R. D., Hinz, P. M., Hoffmann, W. F., Mamajek, E. E., Meyer, M. R., & Hora, J. L. 2002, *ApJ*, 567, L77
- Smith, N., Gehr, R. D., & Krautter, J. 1998, *AJ*, 116, 1332
- Smith, N., & Hartigan, P. 2006, *ApJ*, 638, 1045
- Smith, N., Morse, J. A., Davidson, K., & Humphreys, R. M. 2000, *AJ*, 120, 920
- Smith, N., et al. 2004, *ApJ*, 605, 405
- Soker, N. 2001, *MNRAS*, 325, 584
- . 2004, *ApJ*, 612, 1060
- Stahl, O., Weis, K., Bomans, D. J., Davidson, K., Gull, T. R., & Humphreys, R. M. 2005, *A&A*, 435, 303
- Sugerman, B. E. K., Lawrence, S. S., Crofts, A. P., Bouchet, P., & Heathcote, S. R. 2002, *ApJ*, 572, 209
- Thackeray, A. D. 1951, *Observatory*, 71, 167
- . 1956a, *Observatory*, 76, 103
- . 1956b, *Observatory*, 76, 154
- . 1961, *Observatory*, 81, 99
- ud Doula, A., & Owocki, S. P. 2002, *ApJ*, 576, 413
- van den Bos, W. H. 1928, *Union Obs. Circ.*, 78, 13
- Vishniac, E. T. 1994, *ApJ*, 428, 186
- Visvanathan, N. 1967, *MNRAS*, 135, 275
- Voute, J. C. 1925, *Mem. Bosscha Obs.*, 1, C11
- Walsh, J. R., & Ageorges, N. 2000, *A&A*, 357, 255
- Weigelt, G., et al. 1995, *Rev. Mex. AA Ser. Conf.*, 2, 11
- Young, P. A. 2005, in *ASP Conf. Ser. 332, The Fate of the Most Massive Stars*, ed. R. Humphreys & K. Stanek (San Francisco: ASP), 190
- Zethson, T., Johansson, S., Davidson, K., Humphreys, R. M., Ishibashi, K., & Ebbets, D. 1999, *A&A*, 344, 211